## **OPEN ACCESS**



# Chandra/HETG and NuSTAR Observations of V750 Ara, a $\gamma$ Cas-type Star

David P. Huenemoerder <sup>1</sup> , Sean J. Gunderson <sup>1</sup> , Richard Ignace <sup>2</sup> , Joy S. Nichols <sup>3</sup> , A. M. T. Pollock <sup>4</sup> , Pragati Pradhan <sup>5</sup> , Norbert S. Schulz <sup>1</sup>, Dustin K. Swarm <sup>6</sup> , and José M. Torrejón <sup>7</sup> Kavli Institute for Astrophysics and Space Research, Massachusetts Institute of Technology, 77 Massachusetts Ave., Cambridge, MA 56 02139, USA; dph@mit.edu

Department of Physics & Astronomy, East Tennessee State University, Johnson City, TN 37614, USA
 Harvard & Smithsonian Center for Astrophysics, 60 Garden St., Cambridge, MA 02138, USA
 Department of Physics and Astronomy, University of Sheffield, Hounsfield Road, Sheffield S3 7RH, UK
 Department of Physics and Astronomy, Embry-Riddle Aeronautical University, 3700 Willow Creek Road Prescott, AZ 86301, USA
 Department of Physics and Astronomy, University of Iowa, Iowa City, IA, USA
 Instituto Universitario de Física Aplicada a las Ciencias y las Tecnlogías, Universidad de Alicante, E-03690 Alicante, Spain Received 2025 July 29; revised 2025 October 5; accepted 2025 October 6; published 2025 November 6

#### **Abstract**

We present a 197 ks HETG and 95 ks NuSTAR spectra of the  $\gamma$  Cas-type object V750 Ara. The high-resolution X-ray spectra show that the target is similar to other objects of this class. Data are interpreted under the assumption that the X-rays come from an accreting white dwarf, and our analysis implies an accretion rate of about  $3 \times 10^{-11} \, M_\odot \, \mathrm{yr}^{-1}$ . Emission lines are weak and predominantly from hydrogen-like ions: Mg XII, Si XIV, and S XVI. H-like and He-like Fe are both present, but Fe K fluorescence is weak, being significantly detected only in the NuSTAR spectrum, but it was not obviously detected in the HETG dispersed or zeroth-order spectra. The flux was variable above a level expected by Poisson statistics. There were no significant changes in the spectral hardness, though we are limited by lack of soft signal below 1 keV. Emission lines of Mg and Si were strong enough to measure velocity offsets and widths that were found to be marginally inconsistent. The H-like Mg line is consistent with instrumental broadening only but shows a 300 km s<sup>-1</sup> blueshift. He-like Mg and H-like Si lines have no significant shift in velocity but are broadened by about 1000 km s<sup>-1</sup>. This suggests either different physical origins or velocity structure differing with plasma temperature.

Unified Astronomy Thesaurus concepts: Gamma Cassiopeiae stars (635); High resolution spectroscopy (2096); X-ray astronomy (1810)

# 1. Introduction

There are currently about 25 known stars in the  $\gamma$  Cas-type class (Y. Nazé et al. 2020). They are late O- to early B-type (O9-B3) emission line Oe and Be stars. In the optical and UV, there are no distinguishing features between the  $\gamma$  Cas-type stars and "normal" Oe/Be stars (M. A. Smith et al. 2016; Y. Nazé et al. 2020). In X-rays, however, there is a remarkable difference: the  $\gamma$  Cas-type spectrum is very hard (~10 keV). In embedded wind shock Oand B-stars (that is, excluding colliding-wind systems and Be-Xray binaries with a neutron star), the temperatures are softer at 0.5–1.0 keV. Both the normal stars and the  $\gamma$  Cas-type objects have X-ray emissions consistent with thermal plasmas. The  $\gamma$  Castype stars also sometimes display strong Fe K fluorescence emission, which is not a feature of O- and B-star winds.  $\gamma$  Castype X-ray luminosities (0.5–10 keV) tend to be a bit higher, near 10<sup>32</sup> erg s<sup>-1</sup> (R. Lopes de Oliveira et al. 2006; Y. Nazé & C. Motch 2018; Y. Nazé et al. 2020). Most Be stars, which can have later spectral types than the limit of known  $\gamma$  Cas-type stars, are much less luminous in X-rays (C. Motch et al. 2015).

The number of cases has grown from the eponymous member to enough stars that they now comprise a class. Recent searches for  $\gamma$  Cas-types among Be stars using XMM-Newton has doubled their number (Y. Nazé & C. Motch 2018). Properties of  $\gamma$  Cas itself were reviewed by M. A. Smith et al. (2016), along with a synopsis of about a dozen class members known then. They

Original content from this work may be used under the terms of the Creative Commons Attribution 4.0 licence. Any further distribution of this work must maintain attribution to the author(s) and the title of the work, journal citation and DOI.

speculated on possible origins of the hard X-ray flux, from magnetic reconnection between the star and disk to accretion onto a compact companion. K. Postnov et al. (2017) and M. Tsujimoto et al. (2018) also suggested that  $\gamma$  Cas-type stars' strong X-rays could be due to accretion onto neutron stars or white dwarf (WD) companions. N. Langer et al. (2020) investigated binary star evolution scenarios and found it probable that Be stars have a WD, neutron star, or black hole companion. They suggested  $\gamma$  Cas-type stars are otherwise normal Be stars that have a heliumstar companion whose low mass and low luminosity would make them hard to detect optically, but whose strong wind interactions with the Be star produce the observed high-temperature X-rays. Many of the  $\gamma$  Cas-type stars are now confirmed to be binaries, probably with a low-mass companion  $(0.6-1.0 M_{\odot}; Y. \text{Nazé})$ et al. 2022), but none are known to have main-sequence companions (J. Bodensteiner et al. 2020).

Given the fundamental distinguishing criterion of hard X-ray flux, and the suggestion of the role of binarity and colliding winds, it is important to obtain both broadband and high-resolution X-ray spectra of these stars. The high-resolution characterization of emission lines is needed to resolve gas kinematics. Broadband spectra are needed to constrain plasma temperatures reaching  $\sim\!10\,\text{keV}$  and thereby the implied shock velocities under the hypothesis of colliding winds, wind–disk interaction, or accretion.

Several  $\gamma$  Cas-types have been observed at high resolution with HETG:  $\gamma$  Cas (M. A. Smith et al. 2004; R. Lopes de Oliveira et al. 2010), HD 110432 (BZ Cru; J. M. Torrejón et al. 2012), HD 42054, and  $\pi$  Aqr (D. P. Huenemoerder et al. 2024). They have line widths  $\lesssim\!1000\,{\rm km\,s^{-1}}$ . For a stripped core He-star, wind

**Table 1** V750 Ara Parameters

Property	Value	References
HD	157832	
Spectral Type	B1.5 Ve	(1)
Primary Mass	11 <i>M</i> <sub>☉</sub>	(1)
Secondary Mass	$0.9 \pm 0.1  M_{\odot}$	(4)
	$0.7 - 0.8  M_{\odot}$	(2)
Distance	972 pc	(3)
E(B-V)	0.24	(1)
Projected Rotational Velocity	$220 \ km \ s^{-1}$	(1)
Primary Velocity Amplitude	$6.25 \text{ km s}^{-1}$	(2)
Orbital Inclination	$60^{\circ}$ – $80^{\circ}$	(2)
Orbital Period	95.23 days	(2)
Epoch	2458566.30 HJD	(2)

**Note.** (1) R. Lopes de Oliveira & C. Motch (2011); (2) L. Wang et al. (2023); (3) C. A. L. Bailer-Jones et al. (2021); (4) this work. The epoch is the time of inferior conjunction of the secondary (that is, the secondary is nearest to the observer).

speeds are expected to be  $\sim 2000-3000 \,\mathrm{km \, s^{-1}}$  (J. S. Vink 2017). Hence, widths of  $\sim 1000 \,\mathrm{km \, s^{-1}}$  are compatible with this; the observed line broadening depends on details of wind shock geometry, wind acceleration, relative momentum flux of each wind, shock-cone cooling profile, and viewing angle (D. B. Henley et al. 2003; G. Rauw et al. 2016). For comparison, the embedded wind shock scenario in OB-stars produces temperatures of  $\sim$ 0.3–0.8 keV (3.5–9.0 MK; D. H. Cohen et al. 2021). In the single O4 supergiant,  $\zeta$  Puppis, the maximum temperature is about 1.4 keV (10 MK), equivalent to 900 km s<sup>-1</sup> relative velocity for a strong shock (D. P. Huenemoerder et al. 2020), in a wind with terminal velocity of about 2000 km s<sup>-1</sup> (A. A. C. Sander et al. 2017). In contrast, the massive colliding-wind binary WR 25 has line widths of about 2000 km s<sup>-1</sup>, more comparable to the terminal velocities when observed at an aspect favorable to maximum shock-cone line widths (P. Pradhan et al. 2021).

Based on X-ray spectral and timing characteristics, D. P. Huenemoerder et al. (2024) suggested that  $\pi$  Aqr—and by implication other  $\gamma$  Cas-type stars—host WDs, which are possibly magnetic, and hence the X-ray emission from  $\gamma$  Cas-type stars is similar to that of cataclysmic binaries, a scenario previously proposed by M. Tsujimoto et al. (2023) and R. Klement et al. (2024) .

V750 Ara (HD 157832) was discovered to be a  $\gamma$  Cas-type star with XMM-Newton by R. Lopes de Oliveira & C. Motch (2011) by virtue of a very hard spectrum ( $kT \sim 11 \text{ keV}$ ) for its B1.5Ve spectral type. It was recently determined to be a 95 day period binary by L. Wang et al. (2023) through low-amplitude (6 km s<sup>-1</sup>) periodic radial velocity variations in Balmer  $\alpha$  and  $\beta$  emission lines. They estimated the mass of a companion to be about  $0.75\,M_\odot$ . They did not detect any spectral signature of the companion and tentatively concluded that the companion is too faint to be a subdwarf stripped-envelope O-star (sdO). From He lines in the optical, R. Lopes de Oliveira & C. Motch (2011) found a projected rotational velocity of about 220 km s<sup>-1</sup>. We list stellar parameters for V750 Ara in Table 1.

# 2. Observations and Modeling

We obtained nearly 200 ks of exposure on V750 Ara with the HETG over a period of 20 months, with one 95 ks contemporaneous NuSTAR observation. All data were processed with

**Table 2** V750 Ara Observational Information

ObsID	DATE-OBS (start date)	Exposure (ks)	$\phi_{ m orb}$
27032	2023-02-01T13:10:35	13.60	0.81
27689	2023-02-03T19:59:47	14.58	0.84
27031	2023-09-23T23:37:22	19.70	0.28
27033	2024-01-29T00:36:40	9.44	0.61
29232	2024-01-29T08:11:10	11.59	0.61
29233	2024-01-29T16:17:47	12.30	0.62
29234	2024-01-30T18:27:24	9.24	0.63
30901001002	2024-02-03T19:46:09	95.21	0.67
29374	2024-04-20T16:09:05	25.60	0.48
26494	2024-04-21T11:52:03	14.87	0.49
27034	2024-06-12T18:24:53	17.49	0.04
29448	2024-06-15T23:59:11	17.83	0.07
30463	2024-10-03T23:28:11	17.34	0.22
27035	2024-10-05T14:01:49	13.78	0.24

**Note.** The orbital phase is defined by the ephemeris of L. Wang et al. (2023). The 5-digit ObsIDs are from Chandra, while the 11-digit ObsID refers to NuSTAR.

standard programs for each observatory (CIAO, A. Fruscione et al. 2006; and nuproducts<sup>8</sup>) appropriate to the times of observations. An observation log is given in Table 2.

#### 2.1. Variability and Timing

The source had a relatively constant count rate during the observations. There was excess variance, above that expected for the mean count rate, in both the Chandra and NuSTAR observations. This is a well known phenomenon of  $\gamma$  Cas-type stars and is referred to as "flickering" (A. Bruch 1995, 2021). In Figure 1 we show the NuSTAR light curve for two bin sizes, and the power spectral density (PSD) distribution. The PSD was computed with with the Lomb-Scargle algorithm (J. D. Scargle 1982; J. H. Horne & S. L. Baliunas 1986), as implemented in "isisscripts," a method that is noted for robustly handling unevenly sampled data. The coarsely binned light curve (by 5828 s bin<sup>-1</sup>, the NuSTAR orbital period) clearly shows semiregular excursions that are several times larger than the statistical uncertainties. The PSD shows a clear slope, typical of red noise. To verify the reality of this slope, we also formed the PSD after randomizing the order of rates within the same time bins (hence preserving the window function) and obtained a flat PSD. The Chandra data showed similar fluctuations in their light curves (Figure 1, bottom panel). We detected no large excursions in the count rate or in hardness ratios, though the latter had their sensitivity limited by counting statistics and the effective bandpass.

# 2.2. Spectral Analysis

Since the count rates for both the Chandra and NuSTAR observations were essentially constant, we formed spectra over the entire interval for each instrument. The Chandra count rate was also low enough in the HETG zeroth order ( $\sim 0.03$  count s<sup>-1</sup>) that CCD photon pileup is not an issue, so we also include the zeroth-order spectra. Figure 2 shows the

<sup>8</sup> https://heasarc.gsfc.nasa.gov/docs/software/lheasoft/help/nuproducts.html

http://www.sternwarte.uni-erlangen.de/isis/

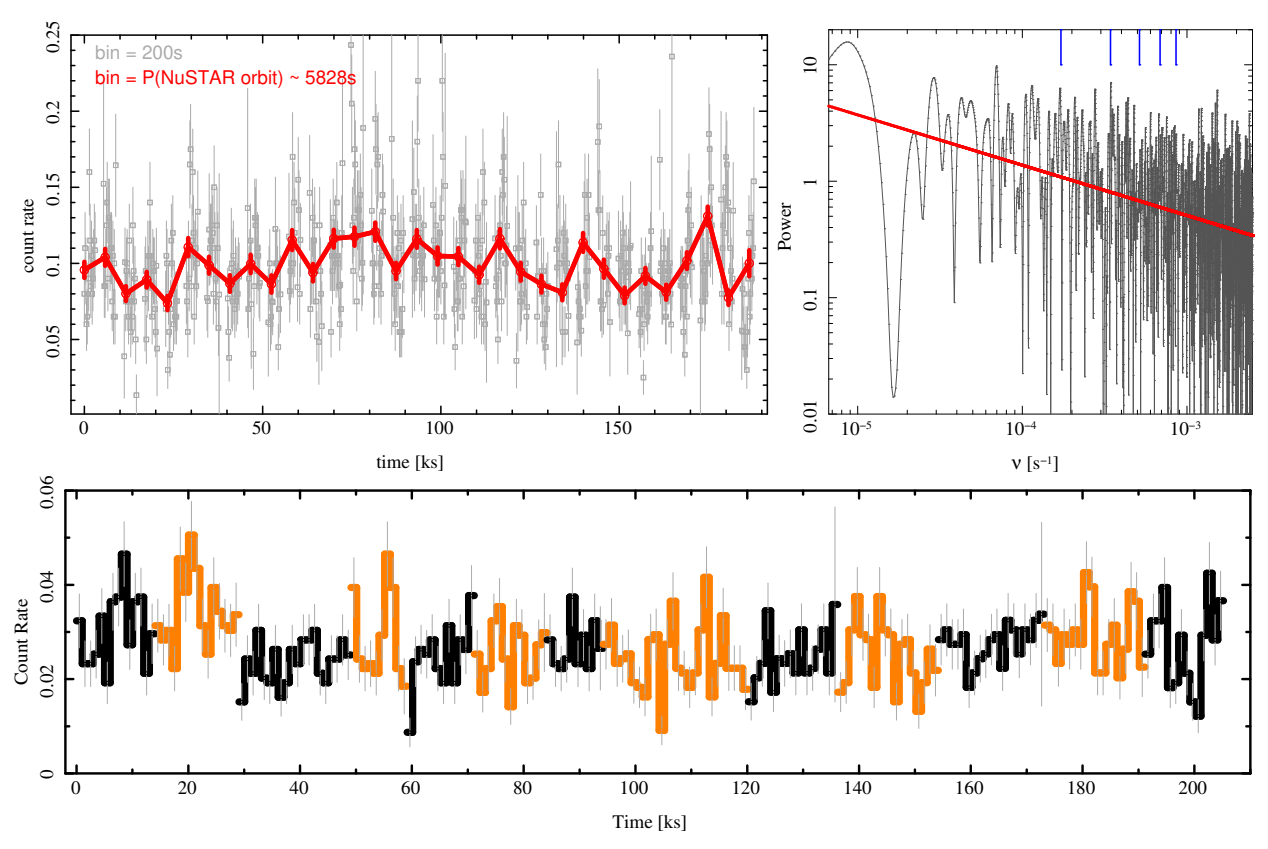


**Figure 1.** NuSTAR light curve (top left) in 200 (gray) and 5828 s bins (red). The larger bin size was chosen to match the period of the NuSTAR orbit. On the top right we show the PSD of the light curve, which shows a slope indicative of red noise, flickering at amplitudes larger than expected from Poisson noise. We did not have enough sensitivity to reach the Poisson noise floor. Blue tick marks at the top indicate the NuSTAR orbital frequency and harmonics, none of which are evident in the transform. Bottom: the HETG light curve of dispersed events in 1 ks bins, with the observations concatenated in time order in alternating colors. The NuSTAR observation is between the two observations at about 95 ks. Count rates are given in s<sup>-1</sup>. The PSD is a unitless normalized probability.

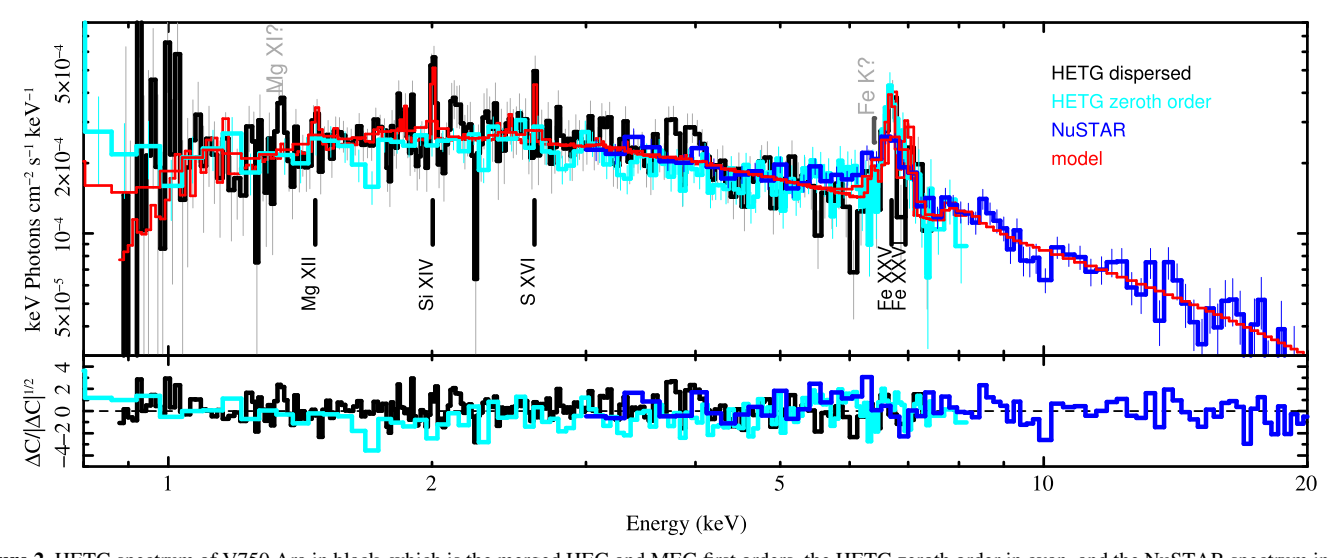


Figure 2. HETG spectrum of V750 Ara in black, which is the merged HEG and MEG first orders, the HETG zeroth order in cyan, and the NuSTAR spectrum in blue (combined FPMA and FPMB). In red is a model using an absorbed cooling-flow model plus a Gaussian for a tentative Fe K fluorescence line. Features with significant detections are marked below the spectrum. The bottom panel shows the residuals in the form of the delta-Cash statistic ( $\Delta C$ ), appropriate for Poisson distributed counts, normalized by its square-root absolute value ( $|\Delta C|^{\frac{1}{2}}$ ), to make it analogous to the commonly used normalized  $\Delta \chi$  statistic. Colors are as in the upper panel.

flux-corrected spectrum for the three cases. No cross-calibration factors were applied. Of particular note is the paucity of emission lines. Mg XII, Si XIV, S XVI, and Fe XXV are significantly detected. Mg XI might be present, while Fe XXVI and Fe K are probably present but relatively weak.

The overall shape is characteristic of a very high-temperature plasma, which is also consistent with the lack of significant lower *Z* and lower-temperature ion states with a narrow range of formation temperature, such as the He-like lines, whereas H-like ions have a long tail of emissivity to high temperatures.

Table 3
Model Fit Results

Parameter	Value	Error	Unit	Comment
norm	1.06	0.06	$10^{-16} M_{\odot} \text{ yr}^{-1} \text{ pc}^{-2}$	
$\dot{M}$	1.0	0.1	$10^{-10} M_{\odot}  \mathrm{yr}^{-1}$	Derived from the <i>norm</i> and distance
$(\gamma)$	0		•••	Cooling-flow exponent; (0 means adiabatic)
$(\log T_{\min})$	6.05	•••	dex [K]	Minimum emission measure temperature
$\log T_{\rm max}$	8.41	0.02	dex [K]	Maximum emission measure temperature
$(v_{\text{turb}})$	600		${\rm km}~{\rm s}^{-1}$	Excess required over thermal broadening
$(\Delta v)$	0			Doppler shift
A(Mg)	1.2	0.3	•••	Abundance factors relative to Solar
A(Si)	1.3	0.2	•••	···
A(S)	1.3	0.4	•••	
A(Fe)	1.3	0.1	•••	•••
$(N_{\rm H}({\rm ISM}))$	0.20	•••	$10^{22}  \mathrm{cm}^{-2}$	Foreground interstellar absorption (R. Lopes de Oliveira & C. Motch 2011)
$N_{ m H}$	0.40	0.02	$10^{22}  \mathrm{cm}^{-2}$	System intrinsic absorption
$f_{\mathbf{x}}$	3.5	0.04	$10^{-12}  \mathrm{erg}  \mathrm{cm}^{-2}  \mathrm{s}^{-1}$	Flux 0.3–20 keV (as observed with absorption)
$L_{\rm x}$	4.1	0.1	$10^{32}  \mathrm{erg \ s^{-1}}$	Luminosity 0.3-20 keV (only the interstellar medium (ISM) absorption was removed)
f(Mg XI)	1.3	0.6	$10^{-6} \text{ photon cm}^{-2} \text{ s}^{-1}$	He-like ion, resonance line
f(Mg XII)	1.0	0.4	$10^{-6}  \text{photon cm}^{-2}  \text{s}^{-1}$	H-like ion, Ly $\alpha$ -like transition
$f(Si\ XIV)$	3.5	0.6	$10^{-6} \text{ photon cm}^{-2} \text{ s}^{-1}$	H-like ion, Ly $\alpha$ -like transition
f(S XVI)	1.4	0.6	$10^{-6} \text{ photon cm}^{-2} \text{ s}^{-1}$	H-like ion, Ly $\alpha$ -like transition
f(Fe K)	1.6	0.5	$10^{-6} \text{ photon cm}^{-2} \text{ s}^{-1}$	Fluorescent emission, joint fit
f(Fe K)	4.0	0.9	$10^{-6} \text{ photon cm}^{-2} \text{ s}^{-1}$	Fluorescent emission, NuSTAR only
f(Fe XXV)	5.6	0.4	$10^{-6} \text{ photon cm}^{-2} \text{ s}^{-1}$	He-like resonance line
f(Fe XXVI)	2.7	0.6	$10^{-6} \text{ photon cm}^{-2} \text{ s}^{-1}$	H-like ion, Ly $\alpha$ -like transition

Note. Parameters in "()" were frozen. Relative abundances are referenced from M. Asplund et al. (2009). The "Error" column gives the one standard deviation uncertainties.  $\dot{M}$  and  $L_{\rm X}$  assumed a distance of 972 pc (C. A. L. Bailer-Jones et al. 2021) and removed only the ISM component of the absorption. Flux and luminosity are integrated from the model over the 0.3–20 keV band. The integrated flux is as observed (uncorrected for any absorption). Line fluxes are from Gaussian fits to each feature, which were the H-like Ly $\alpha$  or the He-like resonance lines, without correction for absorptions.

For a spectral model, we used an absorbed "cooling-flow" model, used in many astrophysical situations, in particular X-ray generation from accretion shocks (D. Pandel et al. 2005; M. Tsujimoto et al. 2018). Our working hypothesis is that the X-ray emission from  $\gamma$  Cas-type stars is likely from a WD companion to the Be star. A cooling flow is a plasma model in which the emission measure distribution (EMD) relative weights as a function of temperature are inversely proportional to the equilibrium plasma cooling time at each temperature. Additionally, the EMD range can be clipped at a high and low temperature outside of which there is no emissivity, and the EMD can be modified by a power-law factor, which represents deviations from an isobaric case. In WD accreting systems, the normalization is proportional to the mass accretion rate, and the maximum temperature is related to the WD mass. Additional model parameters of possible use at high resolution are the line width and velocity offset. For both high- and lowresolution spectra, the elemental abundances are also necessary parameters. G. J. M. Luna et al. (2015) present a thorough overview of the cooling-flow physics and areas of application. Figure 2 shows our best-fit model and residuals. Model parameters are given in Table 3. The cooling-flow model was implemented in the ISIS package (J. C. Houck & L. A. Denicola 2000) using the atomic database (AtomDB) of A. R. Foster et al. (2012) for emissivities and wavelengths.

We also fit features locally with Gaussian profiles folded through the instrument response to investigate any dynamical effects on line widths and centroids. This provides some semiempirical properties independent of global spectral models, though we use the plasma model as a guide for defining Gaussian components and initial parameters. For instance, the H-like lines of Mg XII and Si XIV are doublets with a 2:1 emissivity ratio in

collisionally ionized, low-density plasmas. Using Mg as an example, the separation of the components is about 200 km s<sup>-1</sup>, and the thermal width at maximum emissivity (10 MK) is about 140 km s<sup>-1</sup>, mildly blending the components. However, the HETG instrumental resolution at 8.4 Å is about 700 km s<sup>-1</sup> for the Medium-Energy Gratings (MEG)) or 360 km s<sup>-1</sup> for the High-Energy Gratings (HEG; FWHM of the instrumental profile), much larger than the intrinsic width. Furthermore, the global plasma model indicates that there is additional broadening, which was treated as a turbulent (Gaussian) component in addition to the thermal width, of about  $1000 \, \mathrm{km \, s^{-1}}$ , just resolved by the HETG. Thus, single-Gaussian models are adequate to characterize the H-like emission lines. Even so, at high signal to noise, the single-Gaussian centroid of the H-like doublet is determined by the emissivity-weighted mean position. In referencing the centroid to velocity offsets, we have used the weighted mean positions, though this difference is much smaller than the statistical uncertainties in these observations.

For more crowded regions than those of Si XIV and Mg XII, we included additional components but imposed relative wavelength offsets and used a common width parameter. Such was necessary for the Mg XI and the complicated 6 keV Fe regions. There is also the possibility of unresolved blends, in particular from a host of weak, unresolved dielectronic recombination satellite lines that lie to the low-energy side of the resonance lines. We used the global plasma model and detailed emissivity data in the AtomDB (A. R. Foster et al. 2012) to estimate their flux contribution to a spectral region. For Si XIV and Mg XII, we find only about a 3% contribution, but for Mg XI, Fe XXV, and Fe XXVI, the contribution can be 10%–15%. Fits to the Fe region also included the HETG zeroth-order and NuSTAR spectra, along with the

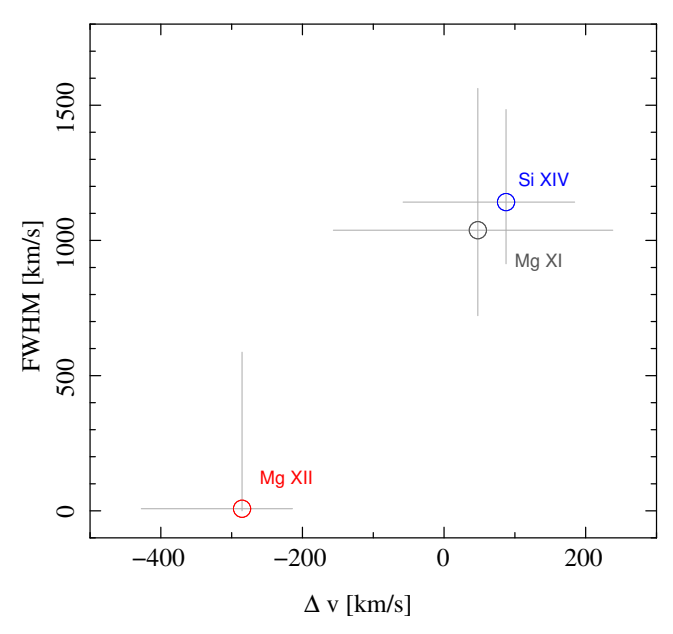


**Figure 3.** Line widths and offsets from Gaussian fits. Only features that provided meaningful constraints are shown. Confidence limits are  $1\sigma$ . H-like feature velocities are in reference to the emissivity-weighted mean of the doublet's wavelengths. The Mg XI He-like resonance, intercombination, and forbidden lines had their relative positions constrained and a common width parameter. Widths are the intrinsic value required in addition to instrumental broadening.

first-order spectrum. Since the Fe K feature seemed present in the NuSTAR data but not in the HETG observation, we have fit the region both jointly in all observations but also in the NuSTAR spectrum alone. The line fluxes are given in Table 3. Line widths and offsets are shown in Figure 3.

## 3. Discussion

The X-ray spectrum of V750 Ara is largely as expected for a  $\gamma$  Cas-type star, namely, thermal, based on line emission, and very hard, characteristic of very high plasma temperatures. The NuSTAR spectrum very strongly constrains the highest temperatures present to about 260 MK (22 keV). This hard component (2–20 keV) also "flickers," showing variance in excess of Poisson statistics (Figure 1), a trait also known among  $\gamma$  Cas stars and common among cataclysmic variables (A. Bruch 2021).

Under the assumption that the X-rays originate from Be star disk accretion onto a WD, the model normalization is proportional to the mass accretion rate, and the maximum temperature is related to the WD mass that controls the accreting plasma's velocity. The normalization (see Table 3) implies  $\dot{M}=10^{-10}\,M_\odot$  yr<sup>-1</sup>, easily within the mass expected to be available from a Be star disk but much less than typical of low-mass X-ray binary Roche overflow rates (J. Patterson & J. C. Raymond 1985a, 1985b). This difference is reasonable, since the reservoir of accreting material is not efficiently funneled onto a WD from a Be star disk. The value is also similar to that of  $\gamma$  Cas (3 ×  $10^{-10}\,M_\odot$  yr<sup>-1</sup>; S. J. Gunderson et al. 2025), despite the different system parameters.

For a WD mass estimate, we can use the relation between maximum temperature, mass, and radius, in conjunction with a nominal WD mass–radius relation (H. Ezuka & M. Ishida 1999), as was done for  $\gamma$  Cas by S. J. Gunderson et al. (2025), to obtain  $M_{\rm WD}=0.9\pm0.1\,M_{\odot}$ . This is consistent with the estimate from the single-lined spectroscopic binary solutions of L. Wang et al.

(2023), who found a mass of  $0.8 M_{\odot}$  if the inclination were  $i = 60^{\circ}$ ; the mass would be larger for lower i. Our values for V750 Ara place it directly on the regression of  $T_{\rm max}$  versus  $M_{\rm WD}$  shown by M. Tsujimoto et al. (2018, their Figure 6).

The emission lines in V750 Ara are quite weak, but we can use the stronger features at the longest wavelengths available in the high-resolution spectrum to constrain flow velocities. Only Si XIV, Mg XII, and a tentative identification of Mg XI are useful, and the width and offset values obtained from Gaussian fits are shown in Figure 3. Widths and offsets are relatively small when compared to strong O-star stellar winds (P. Pradhan et al. 2023) or to sdO winds, which can have velocities of 2000 km s<sup>-</sup> though some are lower (C. S. Jeffery & W. R. Hamann 2010; S. Mereghetti & N. La Palombara 2016). The Mg XI feature is not actually predicted by our plasma model. The tentative identification has a low significance of about  $2\sigma$ . It is our lowest temperature feature and, if real, could be from a cooler component of plasma emission, as was seen in  $\gamma$  Cas by S. J. Gunderson et al. (2025). Here we have moderate absorption and also poor instrumental response to softer X-rays, so we cannot constrain the cooler plasma with these data.

The 6–7 keV Fe-complex shows strong features, mostly due to Fe XXV and Fe XXVI; these are also indicative of the hightemperature plasma. Furthermore, they have line-to-continuum ratios requiring relative abundances of about 1.3 times solar (Table 3), in contrast to  $\gamma$  Cas, which is very subsolar at a relative abundance of 0.33 (M. A. Smith et al. 2004; S. J. Gunderson et al. 2025). The Fe K fluorescent line is not present in the HETG spectrum, though statistics are poor. It does seem required by the NuSTAR data. Hence, we give two flux values in Table 3, one for a joint fit of all data and one for a fit to the NuSTAR spectrum alone. If the  $\gamma$  Cas model of S. J. Gunderson et al. (2025) is scaled to the flux level and iron abundance of V750 Ara, then an Fe K fluorescent line would easily be seen in the HETG spectrum with about twice the flux as determined from our joint fit to the HETG dispersed spectrum, zeroth-order, and NuSTAR spectrum. There are two possible reasons for this. First, the weakness could be indicative of system geometry, which limits our view of fluorescent emission. Second, it could be due to much less dense circumstellar disk material at the WD site. Assuming a stellar radius of  $5R_{\odot}$  for V750 Ara (B1.5Ve), the WD would orbit at  $a_{\rm V750} \approx 40 R_{*}$ ; in contrast,  $\gamma$  Cas companion orbits at  $a_{\gamma} \approx 35 R_{*}$ . The orbital radius ratio is then  $a_{V750} \approx 1.14 a_{\gamma}$ . For a typical Be disk density profile, assuming similar central densities and  $\alpha = 3.5$ , this means  $\rho_{\rm V750} \sim 0.6 \rho_{\gamma}$  at the site of the WD. The line emissivity depends on the plasma density. Thus the line in V750 would be about 2 times weaker than in  $\gamma$  Cas. Furthermore, we have derived a WD mass similar to that of  $\gamma$  Cas. Yet the X-ray luminosity and implied mass accretion rate are a few times lower than  $\gamma$  Cas's values, further reducing the illumination of the reprocessing material. Since scaling the  $\gamma$  Cas line to the V750 flux predicts a strength only a few times greater than what is observed, it is not surprising that we do not detect the line here.

The strength of the line in the NuSTAR spectrum, however, is more than twice the mean value fit jointly over all the spectra and is thus actually consistent with the scaled value of  $\gamma$  Cas. This suggests that the fluorescent line is variable, even though the overall energy distribution of the NuSTAR spectrum agrees nicely with that from HETG.

In short, under this WD accretion hypothesis, these differences are likely indicative of the different Be star disk conditions at the locations of the WD and differences in the Be

star disks due to stellar spectral type and rotation, which change the amount of material available for accretion or the efficiency at which the WD can accrete.

## 4. Conclusions

We have obtained Chandra/HETG X-ray spectra of the  $\gamma$  Cas-type star, V750 Ara, over a time span of almost 2 yr, with one contemporaneous NuSTAR observation. We have interpreted the data in the context of accretion onto a WD companion. While the data do not prove that the companion is a WD, they are consistent with that assumption. The important characteristics are as follows:

- 1. the spectrum is very hard, as born out by the NuSTAR
- 2. spectral features are weak, except for Fe XXV and Fe XXVI, also characteristic of high temperatures;
- 3. X-ray emission lines are slightly broadened, with an intrinsic FWHM of about 1000 km s<sup>-1</sup> larger than instrumental, but not indicative of strong winds (\$\ge 2000 \text{ km s}^{-1}\$) nor of magnetically confined plasmas (unresolved);
- 4. the X-ray flux displays flickering, a trait common in nonmagnetic cataclysmic variables;
- 5. the mean flux and hardness showed no large changes, despite the long coverage; no phase-dependent or discrete absorption events were detected, as have been seen in other systems such as  $\gamma$  Cas (S. J. Gunderson et al. 2025) or  $\pi$  Aqr (D. P. Huenemoerder et al. 2024);
- 6. there may be variable Fe K fluorescence; its reduced mean strength relative to Fe XXV and other  $\gamma$  Cas-type stars must be due to different accretion geometry; yet the NuSTAR data alone contradict this, showing a welldetected feature, consistent with scaled  $\gamma$  Cas flux;
- 7. the mass we derive for the WD is about  $0.9 M_{\odot}$ , consistent with the dynamical estimate of L. Wang et al. (2023) and consistent with the mass–temperature relation shown by M. Tsujimoto et al. (2018).

In summary, V750 Ara, at high resolution, still looks like a  $\gamma$  Cas-type star and is consistent with the companion being a WD.

### Acknowledgments

Support for S.J.G. and D.P.H. was provided the Smithsonian Astrophysical Observatory (SAO) Chandra X-Ray Center (CXC) Award GO3-24004A and by NASA through the SAO contract SV3-73016 to MIT for Support of the CXC and Science Instruments. CXC is operated by SAO for and on behalf of NASA under contract NAS8-03060. S.J.G. and HMG also received support by NASA through Chandra Award Number GO3-24005X issued by the CXC. J.M.T. acknowledges the grant ASFAE/2020/02 from Generalitat Valenciana.

This research has made use of ISIS functions (ISISscripts) provided by ECAP/Remeis observatory and MIT (http:// www.sternwarte.uni-erlangen.de/isis/).

This research employs a list of Chandra datasets, obtained by the Chandra X-ray Observatory, contained in doi:10.25574/cdc.457. Facilities: CXO (HETG), NuSTAR.

Software: CIAO (A. Fruscione et al. 2006), ISIS (J. C. Houck & L. A. Denicola 2000), HEASOFT (https://heasarc.gsfc.nasa. gov/lheasoft/).

```
Huenemoerder et al.
                           ORCID iDs
David P. Huenemoerder https://orcid.org/0000-0002-
3860-6230
Sean J. Gunderson https://orcid.org/0000-0003-2602-6703
Richard Ignace https://orcid.org/0000-0002-7204-5502
Joy S. Nichols https://orcid.org/0000-0003-3298-7455
A. M. T. Pollock https://orcid.org/0000-0002-6737-538X
Pragati Pradhan https://orcid.org/0000-0002-1131-3059
Dustin K. Swarm https://orcid.org/0000-0003-1898-4223
José M. Torrejón https://orcid.org/0000-0002-5967-5163
                            References
Asplund, M., Grevesse, N., Sauval, A. J., & Scott, P. 2009, ARA&A, 47, 481
Bailer-Jones, C. A. L., Rybizki, J., Fouesneau, M., Demleitner, M., &
  Andrae, R. 2021, AJ, 161, 147
Bodensteiner, J., Shenar, T., & Sana, H. 2020, A&A, 641, A42
Bruch, A. 1995, in IAU Coll. 151: Flares and Flashes, ed. J. Greiner,
  H. W. Duerbeck, & R. E. Gershberg (Springer: Berlin), 288
Bruch, A. 2021, MNRAS, 503, 953
Cohen, D. H., Parts, V. V., Doskoch, G. M., et al. 2021, MNRAS, 503, 715
Ezuka, H., & Ishida, M. 1999, ApJS, 120, 277
Foster, A. R., Ji, L., Smith, R. K., & Brickhouse, N. S. 2012, ApJ, 756, 128
Fruscione, A., McDowell, J. C., Allen, G. E., et al. 2006, Proc. SPIE, 6270,
  62701V
Gunderson, S. J., Huenemoerder, D. P., Torrejón, J. M., et al. 2025, ApJ,
Henley, D. B., Stevens, I. R., & Pittard, J. M. 2003, MNRAS, 346, 773
Horne, J. H., & Baliunas, S. L. 1986, ApJ, 302, 757
Houck, J. C., & Denicola, L. A. 2000, in ASP Conf. Ser. 216, Astronomical
   Data Analysis Software and Systems IX, ed. N. Manset, C. Veillet, &
   D. Crabtree (San Francisco, CA: ASP), 591
Huenemoerder, D. P., Ignace, R., Miller, N. A., et al. 2020, ApJ, 893, 52
Huenemoerder, D. P., Pradhan, P., Canizares, C. R., et al. 2024, ApJL,
  966, L23
Jeffery, C. S., & Hamann, W. R. 2010, MNRAS, 404, 1698
Klement, R., Rivinius, T., Gies, D. R., et al. 2024, ApJ, 962, 70
Langer, N., Baade, D., Bodensteiner, J., et al. 2020, A&A, 633, A40
Lopes de Oliveira, R., & Motch, C. 2011, ApJL, 731, L6
Lopes de Oliveira, R., Motch, C., Haberl, F., Negueruela, I., &
  Janot-Pacheco, E. 2006, A&A, 454, 265
Lopes de Oliveira, R., Smith, M. A., & Motch, C. 2010, A&A, 512, A22
Luna, G. J. M., Raymond, J. C., Brickhouse, N. S., Mauche, C. W., &
  Suleimanov, V. 2015, A&A, 578, A15
Mereghetti, S., & La Palombara, N. 2016, AdSpR, 58, 809
Motch, C., Lopes de Oliveira, R., & Smith, M. A. 2015, ApJ, 806, 177
Nazé, Y., & Motch, C. 2018, A&A, 619, A148
Nazé, Y., Motch, C., Rauw, G., et al. 2020, MNRAS, 493, 2511
Nazé, Y., Rauw, G., Czesla, S., Smith, M. A., & Robrade, J. 2022, MNRAS,
Pandel, D., Córdova, F. A., Mason, K. O., & Priedhorsky, W. C. 2005, ApJ,
Patterson, J., & Raymond, J. C. 1985a, ApJ, 292, 535
Patterson, J., & Raymond, J. C. 1985b, ApJ, 292, 550
Postnov, K., Oskinova, L., & Torrejón, J. M. 2017, MNRAS, 465, L119
Pradhan, P., Huenemoerder, D. P., Ignace, R., Nichols, J. S., &
  Pollock, A. M. T. 2023, ApJ, 954, 123
```

Pradhan, P., Huenemoerder, D. P., Ignace, R., Pollock, A. M. T., & Nichols, J. S. 2021, ApJ, 915, 114

Rauw, G., Mossoux, E., & Nazé, Y. 2016, NewA, 43, 70

Sander, A. A. C., Hamann, W. R., Todt, H., Hainich, R., & Shenar, T. 2017, A&A, 603, A86

Scargle, J. D. 1982, ApJ, 263, 835

Smith, M. A., Cohen, D. H., Gu, M. F., et al. 2004, ApJ, 600, 972 Smith, M. A., Lopes de Oliveira, R., & Motch, C. 2016, AdSpR, 58, 782

Torrejón, J. M., Schulz, N. S., & Nowak, M. A. 2012, ApJ, 750, 75

Tsujimoto, M., Hayashi, T., Morihana, K., & Moritani, Y. 2023, PASJ, 75, 177

Tsujimoto, M., Morihana, K., Hayashi, T., & Kitaguchi, T. 2018, PASJ,

Vink, J. S. 2017, A&A, 607, L8

Wang, L., Gies, D. R., Peters, G. J., & Han, Z. 2023, AJ, 165, 203